Physicochem. Probl. Miner. Process., 54(1), 2018, 111-123

Physicochemical Problems of Mineral Processing

www.minproc.pwr.wroc.pl/journal/

ISSN 1643-1049

Received June 12, 2017; reviewed; accepted August 01, 2017

Detailed experimental study of bubble adhesion on hydrophobic surface

Pavlína Basařová, Kateřina Soušková

University of Chemistry and Technology Prague, Department of Chemical Engineering, Technicka 5, 166 28 Praha 6, Czech Rep.

Corresponding author: pavlina.basarova@vscht.cz (Pavlina Basarova)

Abstract: This work is focused on the detailed experimental study of bubble adhesion on a hydrophobic solid surface. The frame rate 16000 fps was used in side view arrangement in order to capture in detail the three-phase contact line expansion and bubble shape changes. Experiments were done in pure water and in solutions of the anionic surfactant sodium dodecyl sulphate in low, medium and high concentrations. It was found out that the rupture of a liquid film is not symmetrical with respect to the vertical axis of the bubble symmetry. This asymmetry of TPC line formation leads to bubble surface oscillations and asymmetry in dynamic contact angles. These dynamic mechanisms are diminished with increasing surfactant concentration. The non-linearity of expansion velocity was also observed. In the case of high bubble surface mobility, the expansion velocity first decreases and after few milliseconds, the second velocity maximum emerges caused by kinetic energy dissipation. In surfactant solutions, the arising Marangoni stresses should be taken into account because the expansion velocity increases in the first moments of TPC line expansion. Existing models, such as hydrodynamic and molecular-kinetic, are not able to incorporate with bubble oscillations in pure liquids as well as the non-monotonic curve of expansion velocity profile in surfactant solutions.

Keywords: *bubble-particle interaction, bubble adhesion, three-phase contact line, surfactant*

1. Introduction

The interaction between bubbles and solid particles is an important mechanism in many industrial processes. The bubble-particle interaction is usually divided into three sub-processes (Yoon, 2000): a collision of bubble and particle, an adhesion and a possible detachment. When the bubble and the particle are sufficiently close together, a liquid interface film is formed between the bubble and the particle surface. The rate of the film depletion (often referred to as film drainage rate) is limited by the liquid viscosity at the beginning of the process, reaching its critical thickness. At this point, the rate starts to be influenced by the intermolecular forces acting between the molecules of the liquid and the solid particle. This phase is the most significant for the selection between hydrophobic and hydrophilic particles. Whereas in the case of hydrophilic surfaces, the intermolecular forces stabilise the liquid interface film so that the bubble never adheres to the solid surface, in the case of hydrophobic surfaces, the forces act to destabilise the film and eventually break it to form the three-phase contact line (Fujasova-Zednikova et al., 2010). The liquid interface film ruptures in the case of highly hydrophobic solid surfaces, but the time of depletion depends on the stability of the film formed, its drainage kinetics and the critical thickness of its rupture (Zawala et al., 2016). Generally, the more hydrophobic the surface is, the less stable the interface film is. Since the hydrophobic surfaces show a high affinity to air, the roughness of the solid surface plays an important role as well because the surface cavities or scratches can entrap air in the form of micro- or nano-bubbles. Zawala et al. (2016) suggested that the presence of air facilitates the film rupture due to the low stability of the local liquid films between the micro- or nano-bubbles and the colliding bubble. The three-phase

http://dx.doi.org/10.5277/ppmp1823

contact (TPC) line in pure water is then formed as a result of coalescence between submicroscopic bubbles already attached to the hydrophobic surfaces and the colliding bubble.

After the rupture of the interface film, the liquid phase begins to retreat from the solid surface due to an uneven distribution of the liquid-gas interfacial tension. The movement of the three-phase contact line is involved in both the wetting and dewetting mechanisms. Dewetting is applied in the case of bubble adhesion on a solid particle, while wetting occurs during liquid drop spreading on a solid surface. The contact line movement is driven by fluid dynamics and molecular interactions of the contacting phases. Surface tension and inertial and viscous forces influence the expansion of the TPC line. The resultant of the forces influences the curvature of the liquid-gas interface and therefore affects the shape of the bubble. The dynamic contact angle is the measure of the interface deformation at the contact point (Phan et al., 2006). The dynamic process of either wetting or dewetting can be described by the velocity of the contact line U which is defined as:

$$U = \frac{dr_{TPC}}{dt}. \tag{1}$$

where r_{TPC} is the radius of the three-phase contact line and t is time. As suggested by Phan et al. (2006), in the case of small bubbles, the bubble surface is assumed to remain axially symmetric with respect to the vertical axis perpendicular to the solid surface, while the centre of the TPC area is stationary during the TPC expansion. Several theoretical models have been developed to describe the TPC line expansion, relating the velocity dependence on dynamic contact angle to measurable properties such as surface and interfacial tension, liquid viscosity and static contact angle. The two main approaches are the hydrodynamic and molecular-kinetic models; the first one is rather macroscopic and discounts the role of the solid surface whereas the second one accommodates it. An alternative view is the combined model, which applies both surface and hydrodynamic factors (Schneemilch et al., 1998).

Cox (1986) established the basics of the hydrodynamic model for the wetting mechanism. It suggests that the process is dominated by the fluid viscous dissipation. Thus, the bulk viscous friction is the main resistance force for the TPC line contact motion (Ranabothu et al., 2005). The theory solves the equations governing the fluid dissipation, the continuity and Navier-Stokes equations, and relates the expansion velocity U to the dynamic contact angle θ. The main deficiency of this model is the description of the fluid motion very near to the contact line. Thus, the slip length of the nanometre scale (characteristic length scale of inner region) was introduced to describe the unique hydrodynamic mechanisms acting in close proximity of the contact line (Phan et al., 2006). The characteristic length scale of a microscopic region is usually of the order of 1 nm. One of the drawbacks of the hydrodynamic model is the means of estimating the microscopic contact angle θ_{micro} since this angle is not readily measurable. In practice the microscopic contact angle is usually replaced by the equilibrium contact angle, which can be experimentally measured (Phan et al., 2003). The velocity of expansion U and the TPC line radius r_{TPC} are given as:

$$U(t) = \frac{\gamma\left(\theta_0^3 - \theta^3(t)\right)}{9\ln(R/L)\,\eta}, \qquad r_{TPC}(t) = \frac{\gamma}{9\ln(R/L)\,\eta}\int_0^t \left(\theta_0^3 - \theta^3(t)\right)dt. \tag{2}$$

where, γ is the liquid surface tension, η is the liquid dynamic viscosity and the ratio R/L is the adjustable parameter. θ_0 is the equilibrium contact angle and θ is the dynamic contact angle. Use of the hydrodynamic theory has been suggested for wetting mechanism at low contact velocities (Ranabothu et al., 2005).

The second theoretical model for wetting and dewetting processes is the molecular-kinetic model. Unlike the hydrodynamic model, it eliminates the viscous dissipation but includes the solid surface characteristics. The theory is based on a statistical treatment of the transport mechanism of molecules and ions. This model assumes the energy dissipation to occur only at the moving contact line, where adsorption and desorption processes occur. The movement of the TPC line is ruled by the statistic kinetics of molecular events arising at the adsorption sites of the solid surface (Phan et al., 2006). The most common approach to the molecular-kinetic model is the one proposed by Blake and Haynes (1969), which is commonly applied to dynamic wetting. The dependence of expansion velocity on the dynamic contact angle is due to the disturbance of adsorption equilibrium, which is driven by the

changes in the local interface tensions (Phan et al., 2003). The equation for the dependence of expansion velocity on dynamic contact angle is given by (Phan et al., 2003 and 2006):

$$U(t) = 2\nu\lambda \sinh\left(\frac{\gamma\lambda^2}{2k_BT}\left(\cos\theta(t) - \cos\theta_0\right)\right). \quad (3)$$

The frequency ν and distance of molecular displacement λ are usually not known, and therefore they have been treated as adjustable parameters. The dimension of λ can be estimated as the order of molecular dimensions (1 nm). The expected value for ν is from 10^{-6} to 10^{-7} s^{-1} (Phan et al., 2006).

Since it was shown that the two mentioned models for wetting and dewetting mechanisms do not fit the entire velocity range of experimental data, a combined molecular-hydrodynamic approach has been proposed (Phan et al., 2003 and 2006, Ranabothu et al., 2005). The dewetting hydrodynamics is used to describe the effect of fluid flow on the interface deformation far from the three-phase contact line. The microscopic contact angle θ_{micro} in the hydrodynamic model is assumed to be dependent on the expansion velocity. Molecular kinetics is then used to determine this contact angle and describe the dewetting close to the contact line. The combined model has been reported as more successful to describe the experimental data than the two previously discussed models for both wetting and dewetting mechanisms by various authors (Schneemilch et al., 1998; Ranabothu et al., 2005; Phan et al., 2006). Recently, Fetzer and Ralston (2009) studied bubble adhesion and investigated the dewetting mechanism of water on surfaces of a wide range of wettability; here the combined model was used to analyse the data. The dewetting mechanism was observed from above assuming the spherical bubble shape and the circular TPC line with the centre remaining in a stable position. The authors reported that on all studied surfaces the contact radius r_{TPC} initially increased quickly and then continuously slowed down until r_{TPC} reached an equilibrium value. Based on asymmetric results for λ found for advancing and receding contact angles, it was concluded that the molecular displacements are not caused by adsorption or desorption events but rather by the nanometre-scale surface heterogeneity (chemical or topographical), which influences the contact line motion in a low-velocity regime.

It is clear from the above overview that all models describing TPC line extension are based on similar principles: *i*) the liquid film break occurs on the bubble symmetry axis; *ii*) the position of the bubble's centre of gravity position is also on the vertical axis of symmetry and *iii*) the radius of TPC line gradually increases as the velocity of TPC line expansion decreases. These assumptions have not yet been experimentally verified. This project is thus focused on the detailed experimental study of bubble adhesion on a hydrophobic solid surface. We use the high-speed camera in side position in high resolution and capture frequency 16,000 fps in order to precisely capture the bubble motion and shape oscillation during the adhesion. The solutions used are demineralized water and solutions of surface active compounds.

2. Material and methods

Experiments were performed at 25 °C in pure water and in an aqueous solution of the anionic surfactant sodium dodecyl sulphate (SDS). The concentrations were 5×10^{-5} M (denoted as SDS low), 3.7×10^{-3} M (SDS medium) and 2×10^{-2} M (SDS high). SDS was purchased from Sigma-Aldrich Chemical Company (for ion pair chromatography, details in Basarova et al., 2017) and used as received. The experimental measurements were performed in a special glass flotation cell (50 cm height, 8 cm width and 6 cm depth). Single bubbles were created by a bubble generator at the top of a thin capillary (inner diameter 10 μm, outer diameter 375 μm; details in Hubicka et al., 2013) and after detaching from the capillary the bubble rose through the liquid to the solid particle represented by a silanized glass placed on a horizontal plane. The distance between the capillary tip and the glass surface was 20 cm and the bubbles reached the terminal rising velocity. The mechanism of bubble-particle interaction, i.e. the bubble motion before the collision with the solid particle and during the adhesion, was recorded using a high-speed digital camera Photron FastCam SA1.1 (16000 fps, resolution of 768×512 pixels) with a Navitar macro objective. Silanized glass was used as a model hydrophobic surface. The Silanization solution I was supplied by Sigma-Aldrich (5% solution of dimethyldichlorosilane in heptane, CAS No. 75-78-5). The glass material (microscopic slides) was cleaned in a boiling mixture of sulphuric acid and hydrogen peroxide (1:1) for 1 min, then rinsed several times with distilled water

and dried. The slides were dipped into the silanization solution for 24 h then rinsed firstly with pure heptane, then with acetone and ethanol in order to remove all organic residues, and finally, they were dried. The contact angle for pure water drops was 98.2°.

At least five video sequences were captured for every size of the bubble. The image analysis was done using the NIS-Elements Advanced Research software. The video series were converted to the nd2 format and saved with the relevant calibration (approx. 2.8 μm per pixel). All the sequences were qualitatively observed with regard to possible bouncing, bubble shape deformation and the symmetry of three-phase contact line expansion. The bubble diameter D_b, the time of liquid interface film depletion t_{dep} and the final equilibrium contact angle θ_0 were measured for every sequence. The development of the diameter of TPC line d_{TPC} over time was evaluated for each sequence as well. The dynamic contact angle θ and the position of bubble gravity centre changing with time were evaluated only for one selected sequence for each experimental solution since these analyses were time demanding due to the length of the processed sequences (5000 frames). The software functions centreX and centreY were used for the determination of bubble centre. The velocity of TPC expansion was calculated as:

$$U_i = \frac{d_{TPC}(t_{i+1}) - d_{TPC}(t_i)}{2 \cdot (t_{i+1} - t_i)}. \tag{4}$$

The dynamic surface tension of all solutions at 25 °C was measured using the Krűss tensiometer BP100 employing the maximum bubble pressure method. It characterises the adsorption of surface-active molecules on a liquid-gas interface. The maximum bubble pressure measurement method gives the dependence of surface tension on surface age. The surface tension of water at 25 °C is 72.4 $mN \cdot m^{-1}$ and does not depend on the bubble age (see Fig. 1). In solutions of surfactants, the surface tension changes over time. A freshly formed liquid-gas interface has a surface tension very close to that of a solvent. Over a period of time, surface-active molecules adsorb onto the interface. The surface tension decays to its equilibrium value and this period of time can range from milliseconds to days depending on the surfactant type and concentration. SDS has a simple molecule, it adsorbs fast from the subsurface to the interface and the diffusion-controlled adsorption model could be used for its description (Basarova et al., 2017). The decrease of surface tension is evident already after 10 ms of surface age as seen in Fig. 1, except for a lowest concentration of SDS, where the decrease is observable at a surface age of 80 ms. The measurement was limited to a surface age of 100 s and both solutions with low SDS concentrations and high SDS concentrations reached their equilibrium surface tension whereas, in the case of medium SDS concentration, the surface tension is further expected to slightly decrease. The surface tension of all studied solutions is sufficiently different and thus the influence of surface active agents on bubble adhesion dynamics could be discussed for low, medium and high surfactant concentration.

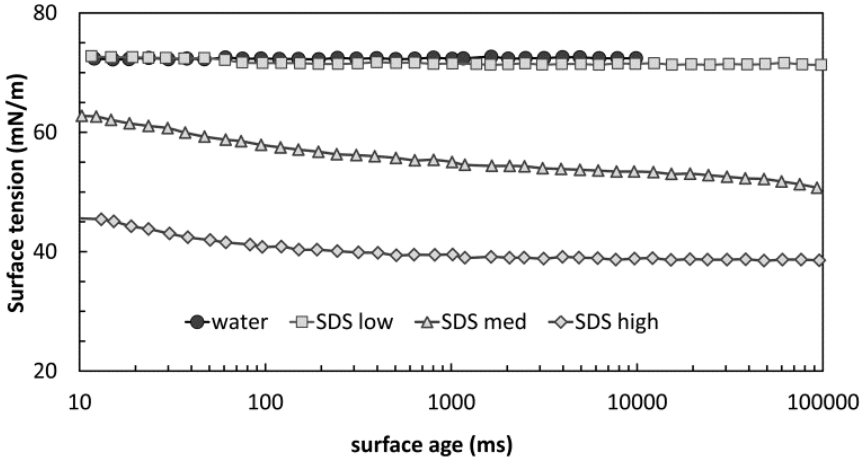

Fig. 1. Dynamic surface tension measured by maximum bubble pressure method. Concentrations of SDS solutions are 5×10^{-5} M (SDS low), 3.7×10^{-3} M (SDS medium) and 2×10^{-2} M (SDS high)

3. Results and discussion

The bubble adhesion was captured by a high-speed camera at 16,000 fps and about 5,000 frames were saved for each image sequence. That captures around 300 milliseconds of the process within which the bubble collided with the solid surface, the interface film formed, depleted and ruptured and the three-phase contact line expanded to equilibrium. Each of these steps had a distinct behaviour for different surfactant concentrations. The characteristics of bubble adhesion onto hydrophobic silanized glass in water and each SDS solution are thus discussed separately.

3.1 Pure water

Figure 2 shows the different steps of bubble interaction (D_b = 0.705 mm) with a particle of infinite radius and a hydrophobic surface. The bubble rises in the solution towards the solid particle (WC1) and it collides with the particle (WC2). After the collision, the bubble is deformed; higher speed leads to a bounce (WC3), in some cases, even to multiple bounces. Subsequently, the bubble returns to its own original shape and a liquid film is created between the bubble and the particle (WC4) (the film itself is usually not visible on the captured images because of the pixel resolution, wavy character of light and aperture angle). The film gradually depletes and ruptures. Image W0 illustrates the situation just before the film rupture. Note that this time (t = 0 ms) is set as the time of the rupture of the liquid interface film, therefore the images capturing the bubble-particle collision and liquid interface film depletion are indicated with negative times. The formation of the three-phase contact (TPC) line is visible after 0.0625 seconds (W1). The TPC line expansion continues (W2) together with significant bubble shape deformation, where the bubble is first prolonged (W3, W4) and then compressed (W5 - W7) in the vertical direction. While the diameter of the three-phase contact line does not change significantly anymore, the bubble shape deformation is still observable (W8 - W10). The bubble shape deformation during expansion could be described as a form of bouncing while keeping the three-phase contact. We assume that this is caused by residual kinetic energy dissipation and full bubble surface mobility which allows the interfacial oscillations and waves on bubble surface. Image W11 presents the bubble at equilibrium, where both the diameter of the TPC line and the bubble shape do not change anymore.

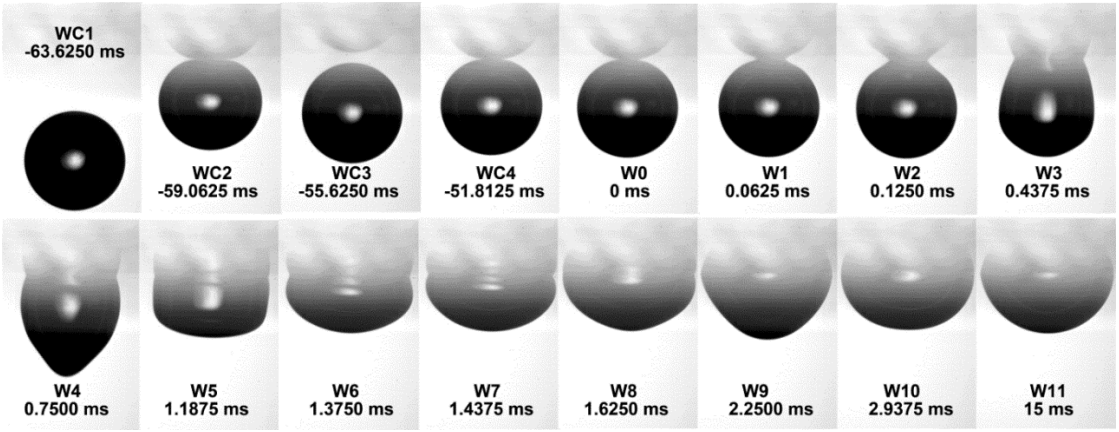

Fig. 2. A series of photos illustrating a course and outcome of the bubble (D_b = 0.705 mm) adhesion onto the solid surface in pure water

The bubble movement described above can be quantified as the position of the bubble gravity centre changing with time. Figure 3A shows the relative change of the bubble gravity centre position (centre Y) in the vertical direction over time. Note that the Y coordinate increases opposite to the bubble movement as shown in Fig. 2 and in this graph, this value is normalised by the position at t = 0 milliseconds. Both the above discussed bouncing after the bubble-particle collision and the bubble shape deformation during the TPC line expansion can be represented by the sinusoidal parts of the graph. The bubble gravity centre motion during the first moments of the TPC line expansion is shown in more detail in Fig. 3B.

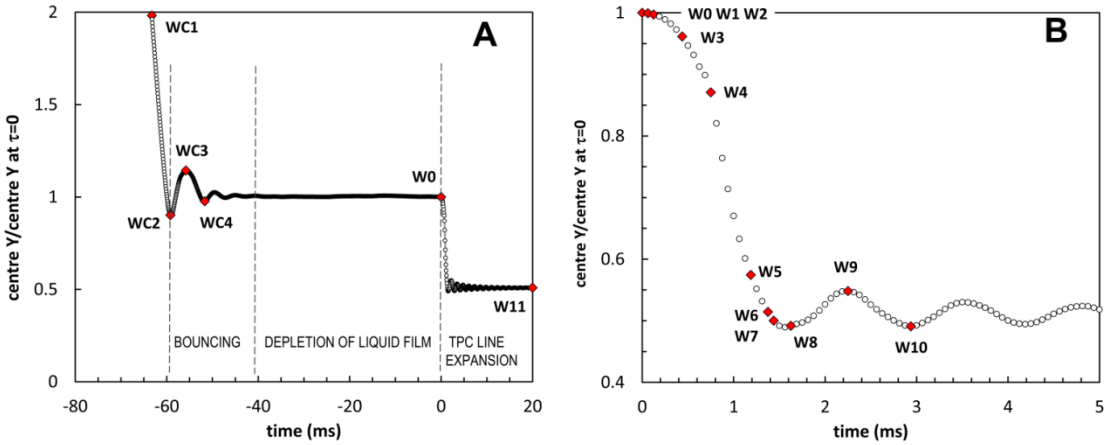

Fig. 3. The bubble gravity centre's motion in the vertical direction. The highlighted points correspond to images in Fig. 2

The diameter of the three-phase contact line d_{TPC} was measured for every image of the video sequence and the expansion velocity U was calculated in each time step according to eq. 4. The time dependence of both quantities for the individual bubble to before is shown in Fig. 4A. The non-zero value of d_{TPC} at t = 0 ms does not have a physical meaning as the three-phase contact is not formed yet. The TPC line in water expands very quickly; the velocity reaches its maximum (almost 0.5 m·s^{-1}) in the first captured moment (the visible change between images W1/W2). The TPC line continues to grow but with a decreasing velocity. At around 1.3 ms the expansion velocity increases again and its peak is observable with its maximum at 1.375 ms (the change between images W6/W7). We assume that this acceleration is caused by the bubble shape deformation. As the bubble is being compressed (W6 and W7 in Fig. 2), the bubble mass is forced to shift to the horizontal direction, therefore the three-phase contact line expands faster. As the TPC line diameter reaches a stable value, the expansion velocity becomes zero (W8). Even though the bubble shape continues to change after this point, it does not affect the size of TPC line significantly anymore. Figure 4B shows the expansion velocity for different bubble sizes in water. The points represent the average value measured from 5-6 sequences. Although it seems that the bubble size does not actually influence the extent of the velocity, as both peaks are of the same height for different bubble diameters, it significantly influences the timing. The smaller the bubble, the earlier the velocity peak appears and the earlier the equilibrium diameter (zero velocity) is reached. Individual bubble behaviour was observed and mathematically described by Zawala et al. (2016). To conclude, typical features of bubble adhesion in pure water are *i*) visible bouncing after the collision, *ii*) fast TPC line expansion (finished in 2 ms), *iii*) bubble shape deformation during the adhesion and *iv*) additional maximum on velocity profile.

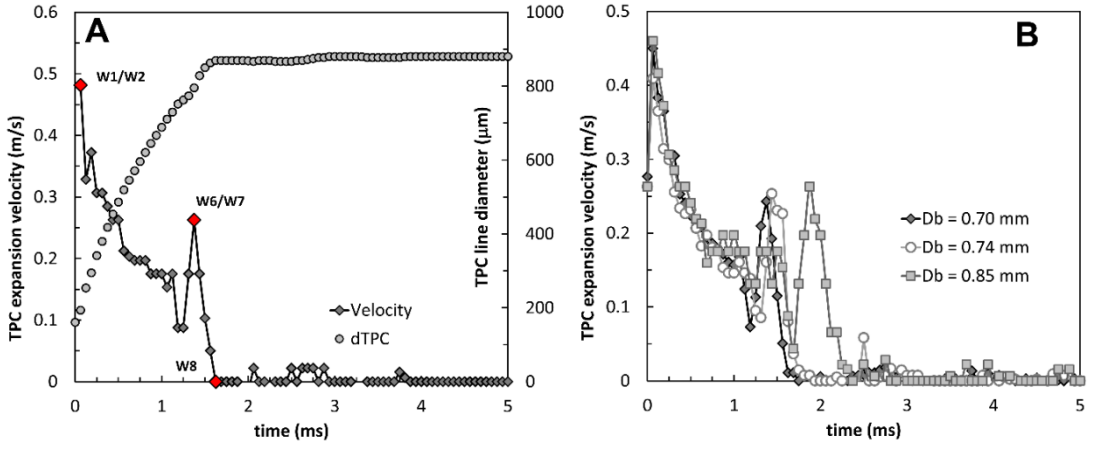

Fig. 4. TPC expansion velocity and diameter of the TPC line expansion in pure water for a bubble with diameter 0.705 mm (detail A) and average values for bubbles with diameters 0.70 mm, 0.74 mm and 0.85 mm (detail B)

The time-dependence pattern of dynamic contact angles matches the course of d_{TPC} (Fig. 4A). Firstly we observed a fast increase of contact angle values and then, after 1 ms, we observed the oscillations between left and right angles reaching up to 6°. Only insignificant increase was observed after 3 ms which goes together with negligible TPC expansion velocity. The average equilibrium contact angle was 98° and this value did not change with changing bubble size.

3.2 Solutions with low surfactant concentration

Figure 5 illustrates the bubble adhesion process (D_b = 0.865 mm) in a solution of a very low concentration of SDS (5×10^{-5} M). It shows representative images of bubble adhesion at indicated times before (SLC1-SL0) and after (SL1-SL10) the liquid interface film rupture. The bubble gravity centre movement in the vertical direction is shown in Fig. 6A. The bubble rises in the surfactant solution (SLC1), it collides with the solid surface, the bubble shape being deformed (SLC2), and it slightly rebounds (SLC3) before colliding with the solid surface again (SLC4). This phase does not differ significantly from the collision behaviour in pure water; therefore, we can assume that the leading pole of the bubble is completely free of surfactant molecules, which seems to be a reasonable assumption considering the very low surfactant concentration. The three phase contact line forming from the right side can be observed (with a close look) in image SL1. Afterwards, the TPC line continues to expand only on the right side (SL2). The left side of the TPC line starts to move after another 0.5 milliseconds. A slight bubble shape deformation is visible (SL4, SL5) and an oscillation of the bubble gravity centre is observed (Fig. 6B). When compared with the results for pure water (see Fig. 3), we can observe a substantial suppression and time extension of the bubble oscillations in the vertical direction. This behaviour is typical for solutions with low surfactant concentration.

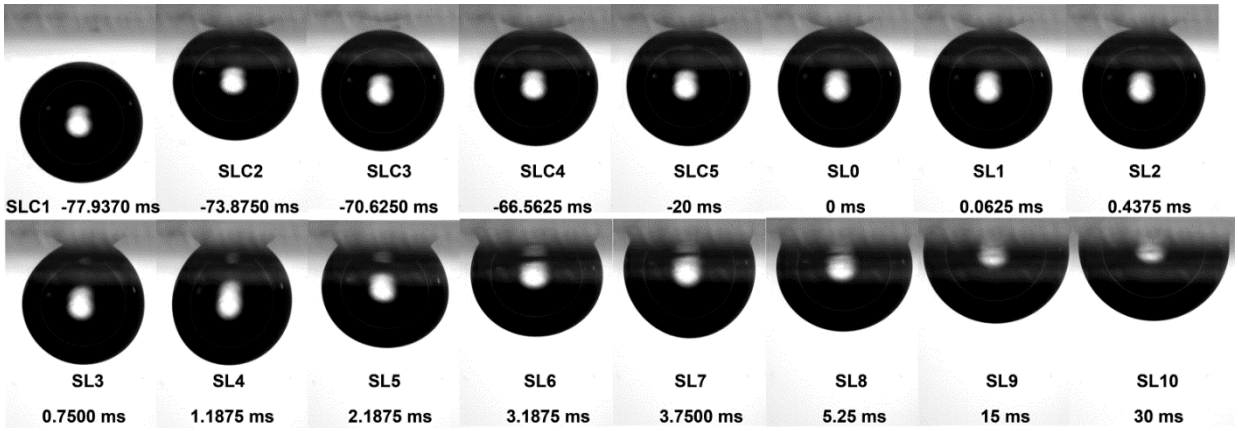

Fig. 5. Sequence of photos illustrating a course and outcome of the bubble (D_b = 0.865 mm) adhesion onto the solid surface in aqueous solution of SDS (low concentration 5×10^{-5} M)

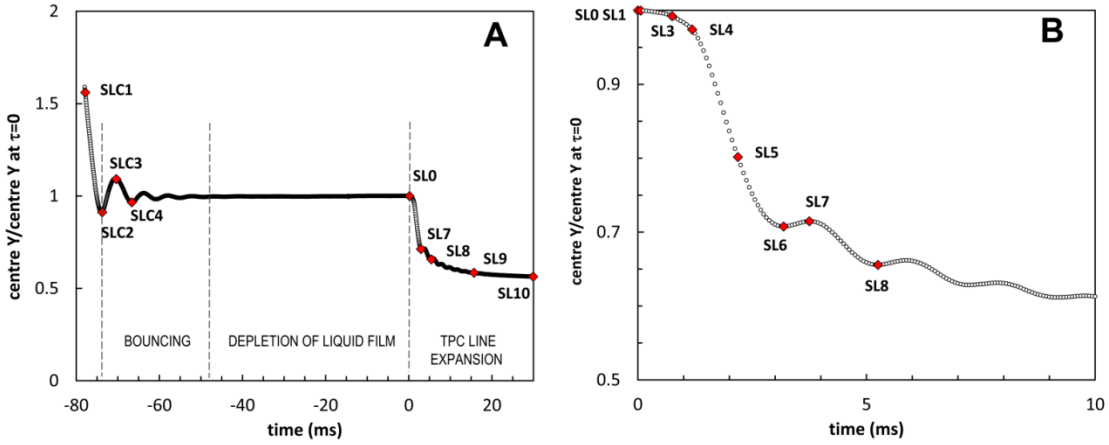

Fig. 6. The bubble gravity centre motion in the vertical direction in an aqueous solution of SDS (low concentration 5×10^{-5} M). The highlighted points correspond to the images in Fig. 5

The fact that the TPC line expansion does not start at the centre of the bubble contact and that the expansion is not symmetric was observed in many image sequences of all the studied solutions, including pure water. In fact, the TPC line expansion started from the centre only in less than 20% of cases. We assume that the positioning of the liquid interface film rupture is related to the inhomogeneity given by the presence of microscopic bubbles and solid surface roughness (Krasowska and Malysa, 2007). During these oscillations, dynamic contact angles measured on right and left side of the bubble vary by 6°.

The time dependence of both the diameter of three-phase contact line and the expansion velocity U for the individual bubble is shown in Fig.7A. The TPC line expansion accelerates (SL2) after 0.5 ms. The velocity then reaches its maximum after 1 ms of expansion (SL4). After 2 ms a second peak can be noticed (SL5), but this is in no case as significant as in water. This is in agreement with the previously made conclusion that the second peak is caused by a bubble shape deformation. The expansion comes to a slow phase around 3.5 ms (SL7). After this point the TPC line diameter increases very slowly and taking into account the pixel resolution and calibration, the measurable change in d_{TPC} is not observed at each time step and therefore the expansion velocity U appears to fluctuate even though the actual velocity is gradually decreasing to zero. Image SL10 shows the bubble after reaching the three-phase contact equilibrium. Figure 7B shows the expansion velocity for two bubble sizes. Similarly to the results in pure water, one can observe an influence of bubble size. The position of the second peak of velocity maximum was observed earlier for the smaller bubble. Moreover, we observed the different initial expansion velocity, which was probably influenced by the different surfactant coverage of the bubble surface due to the different bubble size. When compared with pure water, the velocity of the TPC line expansion has dropped to roughly half and thus the adhesion time has increased. The average equilibrium contact angle was 94° and this value did not depend on bubble size. The typical features of bubble adhesion are: i) a moderate bubble shape deformation during the adhesion and ii) two maxima in the velocity profile.

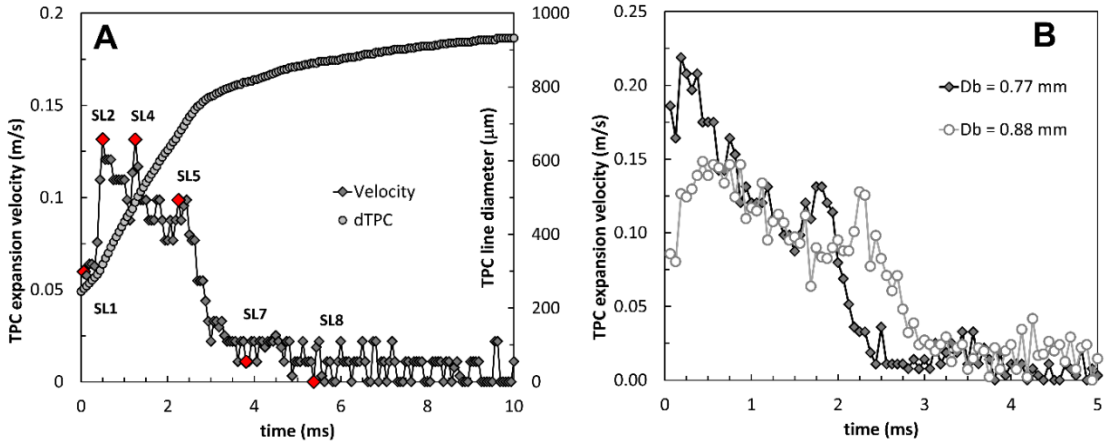

Fig. 7. TPC expansion velocity and diameter of TPC line expansion for a bubble with diameter 0.865 mm (detail A) and average values for bubbles with diameters 0.77 mm and 0.88 mm (detail B). Low SDS concentration

3.3 Solutions with medium surfactant concentration

Figure 8 shows the different steps of bubble adhesion (D_b = 0.926 mm) onto the hydrophobic surface in the aqueous solution of SDS with the concentration 3.7×10^{-3} M. This surfactant concentration is still below its critical micelle concentration. The figure shows representative images of the bubble adhesion at indicated times before (SMC1-SM0) and after (SM1-SM6) the liquid interface film rupture.

The bubble gravity centre movement in the Y direction (centre Y normalised by the centre Y at t = 0) is shown in Figure 9. The bubble rises towards the solid particle (SMC1) and collides, the bubble shape being deformed (SMC2). The bouncing is limited; the bubble moves back from the surface only slightly (SMC3) as seen on the bubble gravity centre movement. This motion is influenced by the presence of surfactant molecules, which decreases the surface elasticity. The liquid interface film ruptures (SM0) and the three-phase contact line starts to expand. The expansion starts on the left side

(SM1, SM2) and the right side expands after another 1.5 ms (see Fig. 9B). The bubble shape deformation (SM3) is thus caused by the non-symmetry of the expansion. The effect of the non-symmetrical TPC line expansion on the dynamic contact angles is crucial and the contact angles on the left and right side can vary by up to 5 degrees. Later, only small oscillations are observable in the vertical movement of the bubble gravity centre (SM4) and the bubble centre reaches its stable position after 15 ms (SM5, SM6) as seen in Fig. 9B. The motion in the horizontal direction follows due to the inertial force. Please note the different magnitudes of the main and minor vertical axes. Whereas the distance between SM2 and SM4 position in the vertical direction is 100 μm, the same distance in the horizontal direction is only 30 μm. A similar horizontal motion of bubble centre was observed for majority of bubbles. The displacement of bubble centre in water did not exceed 20 μm, while in SDS solutions the average horizontal distance ranged from 30 to 40 μm.

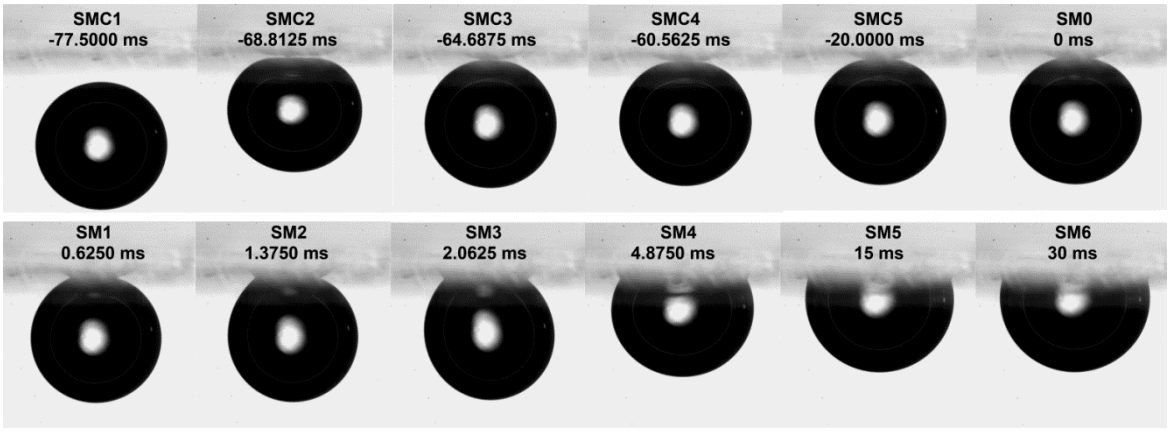

Fig. 8. Sequence of photos illustrating a course and outcome of the bubble (D_b = 0.926 mm) adhesion onto the solid surface in aqueous solution of SDS (medium concentration 3.7×10^{-3} M)

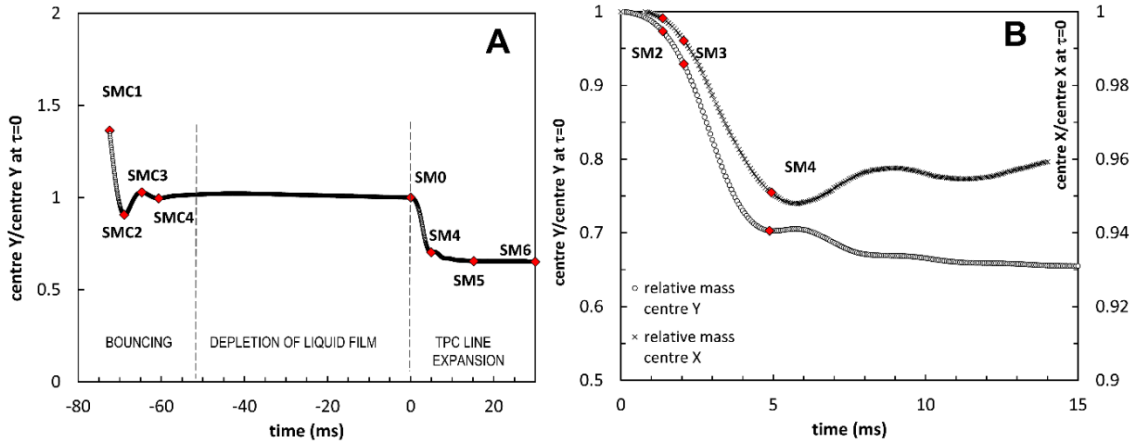

Fig. 9. The bubble gravity centre motion in the vertical direction in aqueous solution of SDS (medium concentration 3.7×10^{-3} M). Detail B: the relative vertical and horizontal bubble gravity centres motion after the TPC line formation. The highlighted points correspond to the images in Fig. 8

The progress of the TPC line diameter and the expansion velocity is shown in Figure 10A. The diameter expands slowly in the first millisecond, then the expansion velocity increases and the TPC line expands at a maximum velocity around 2 ms after the liquid film rupture (SM2, SM3). Afterwards, the expansion velocity decreases and it comes to a slow phase around 5 ms (SM4). The second increase of the expansion velocity is visible only for the biggest bubble at 4 ms. Data for three bubble sizes are summarised in detail B. The course of velocity is similar for all studied bubbles. The velocity decreases significantly up to 0.1 m·s^{-1} maximum and the adhesion time is prolonged to 10 ms. The dynamic contact angles increase gradually following the pattern of d_{TPC}. The average equilibrium contact angle was 82^{o}. By analysing all the image sequences captured for medium SDS concentration it

can be concluded that the typical features of bubble adhesion to hydrophobic surface in SDS concentration below CMC are: *i*) a hindered bouncing after the collision due to presence of surfactant molecules, *ii*) an asymmetric rupture of the liquid interface film (the TPC line expands at one side), and *iii*) an expansion velocity increase within the first moments of the TPC line expansion and its maximum at 1.5 ms.

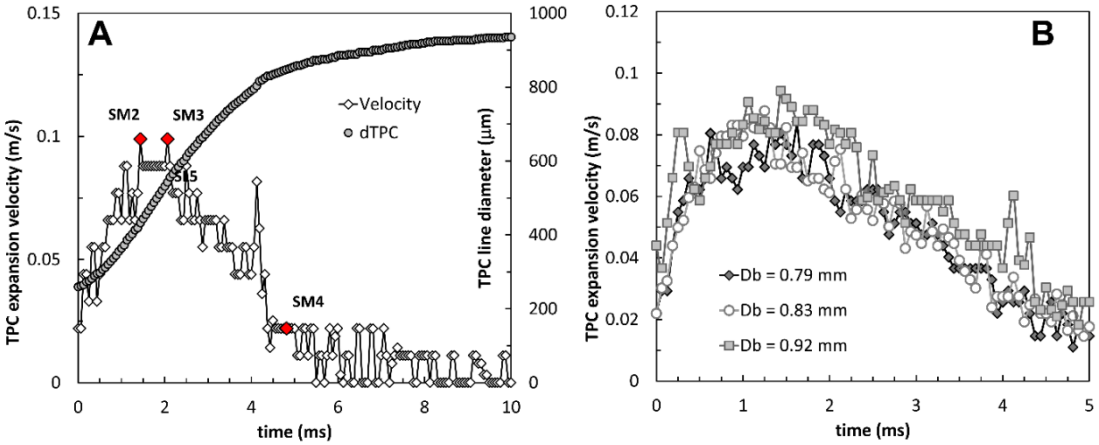

Fig. 10. Bubble velocity and diameter of the TPC line expansion for a bubble with diameter 0.926 mm (detail A) and average values for bubbles with diameters 0.79 mm, 0.83 mm and 0.92 mm (detail B). Medium SDS concentration

3.4 Solutions with medium surfactant concentration

Figure 11 illustrates the bubble adhesion process (D_b = 0.864 mm) in a solution with high concentration of SDS (2×10^{-2} M), which is above the critical micelle concentration. It shows representative images of the bubble adhesion at indicated times before (SHC1-SH0) and after (SH1-SH5) the liquid interface film rupture.

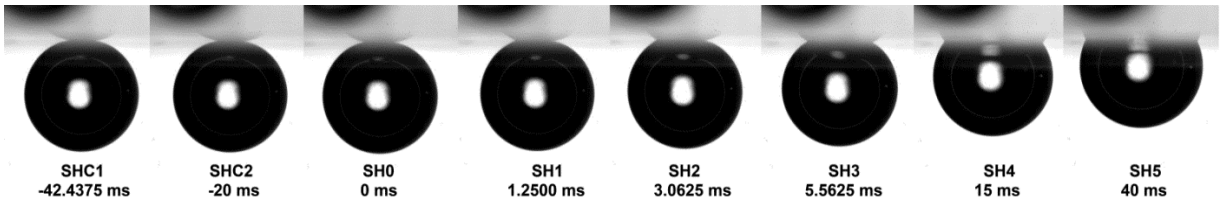

Fig. 11. Sequence of photos illustrating a course and outcome of the bubble (D_b = 0.864 mm) adhesion onto the solid surface in aqueous solution of SDS (high concentration 2×10^{-2} M).

The bubble gravity centre movement in the Y direction (centre Y normalised by the centre Y at t = 0) is shown in Fig. 12. The bubble rising and its collision with the solid surface was not captured because the time lapse between the collision and the actual formation of the TPC line was longer than is possible to capture; it varied between 5 and 30 seconds. No bubble bouncing was observed (SHC1, SHC2). The extended time of the liquid interface film depletion is caused by the high concentration of surfactant molecules, which stabilises the interface film (Malysa et al., 2005). The variation in the depletion time could be caused by a different distribution of microscopic bubbles, which corresponds to the distribution of surface imperfections. The image SH0 shows the bubble right before the rupture of the interface film. The TPC line then starts to expand from the left side (SH1), the right side slowly joining only after 2 ms. The bubble regains symmetry after 5 ms (SH3) and slowly continues to expand. The expansion is still not finished after 15 ms (SH4) and the equilibrium TPC line diameter is reached only after 40 ms (SH5). No bubble shape deformation is detected and the bubble centre moves steadily towards the solid surface. The high concentration of surface active molecules in the solution is assumed to result in the bubble being completely covered by surfactant molecules. The adsorption and desorption exchange of the surfactant molecules between the bubble and the solid surface then

control the rate of the TPC line expansion. The time-dependence of the expansion velocity U is shown in Fig. 12. The expansion of the TPC line is similar to that of Fig 10A and it is even more gradual. Since the expansion is very slow and the TPC line diameter changes only within a few μm between the two images, the expansion velocity was calculated over a longer time step 0.5 ms to better capture the actual progress of the expansion velocity. The expansion velocity increases during the first 3 ms of the expansion when it reaches its maximum (SH2). Afterwards, the expansion starts to slow down at 6 ms and slow phase is reached after approximately 20 ms of expansion.

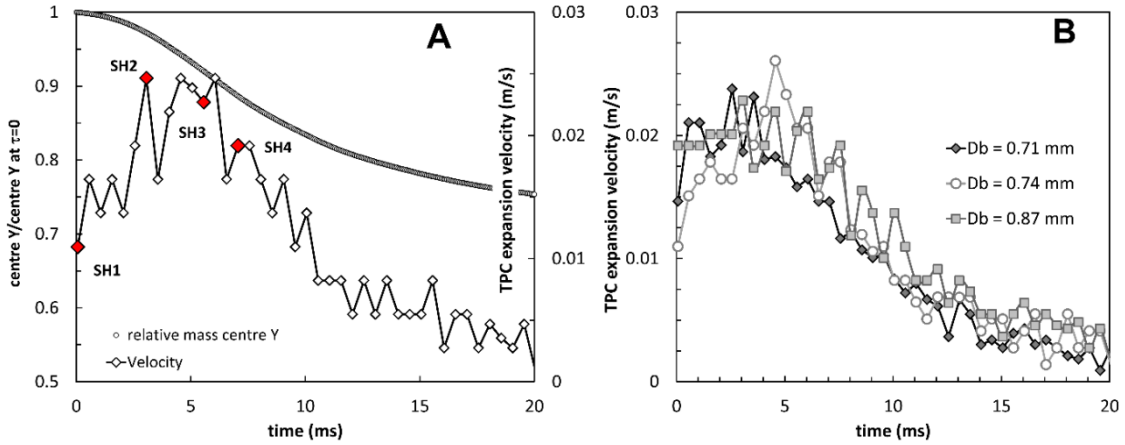

Fig.12. TPC expansion velocity and the relative bubble gravity centre motion in the vertical direction for a bubble with diameter 0.864 mm (detail A) and average values for bubbles with diameters 0.71 mm, 0.74 mm and 0.87 mm (detail B). High SDS concentration

Data for three bubble sizes are summarised in detail B. The course of velocity is similar for all studied bubbles. The maximum value 0.02 m·s^{-1} was reached after 5 ms and the whole adhesion time prolonged to more than 20 ms. The average equilibrium contact angle was 69° and its value did not depend on bubble size. The typical features of bubble adhesion in a high concentration of surfactant are: i) no bouncing after the collision or during the bubble adhesion, ii) liquid film stabilisation and iii) a very slow TPC line expansion.

3.5. Applicability of existing theoretical models

The hydrodynamic and the molecular-kinetic models are two alternative approaches usually used for the description of the bubble TPC line expansion. In both cases, the driving force of this process is the difference between the dynamic and the equilibrium contact angles (Eqs. 2 and 3). The suitability of these models has been investigated by many researchers and the bubble adhesion process was observed either from the side view or from above, but with relatively low image frame rate. The limited frame rate did not allow direct calculation of expansion velocity and most of the papers studied the dependency of the TPC line radius on the dynamic contact angles. The studies also assumed that in the case of small bubbles (D_b < 1 mm), the bubble surface remains axially symmetric and the radial position of the TPC line is equal to the radius r_{TPC}. Moreover, demineralized water was used as a liquid medium in all of the published works. None of these models can deal with a liquid containing surfactants.

This work offers a new opportunity to observe the bubble adhesion process in a very detailed experimental study and thus it offers the comparison of the above-mentioned theoretical assumptions with the reality. Bubble adhesion in pure water and in solutions of surface-active agents was described in detail in the previous chapters. The main experimental observations can be summarised in the following points:

i) The rupture of a liquid film is not symmetrical with respect to the vertical axis of the bubble symmetry. This finding is in accordance with the conclusion of Chan et al. (2011), who proved that the liquid film becomes the thinnest close to the apparent contact line.

ii) The asymmetry of the TPC line formation leads to bubble surface oscillations and asymmetry in dynamic contact angles. For mobile surfaces, the uneven motion of the TPC line causes the change of boundary conditions. Due to the gradual kinetic energy dissipation, we can observe bubble shape oscillations both in the vertical and horizontal direction. Similar linear oscillations and irrotational flow during the bubble contact with the solid surface were described by Vejrazka et al. (2013). When surface-active agents are captured at the liquid-gas interface, the viscoelasticity of the bubble surface decreases significantly and the shape oscillations are dampened.
iii) The expansion velocity increases in the first moments of the TPC line expansion and in a case of a high surface mobility we can observe a second velocity maximum. The increase of expansion velocity after the TPC line formation was observed in solutions with surface-active agents. Due to a sufficient time interval between the bubble collision with the surface and the creation of the TPC contact, we expect the bubble surface to be uniformly covered by surfactant molecules. After the TPC line creation, the arising Marangoni stresses should be taken into account. The pure water-air interface is mobile and cannot withstand shear stress tangential to the air-water interface. In the presence of surfactants, the situation changes because gradients in the surface excess of surfactants can cause an effective no-slip boundary condition. At the TPC line, the solid-liquid and the air-liquid interfaces merge. In close proximity, where the distance between the solid-liquid and the liquid-vapour interface is below 100 nm, the surface force acts between the two interfaces. Merging would be delayed if a long-range repulsive surface force acted between the interfaces. Here, the charged head groups of the surfactants adsorbed at both interfaces would lead to an electrostatic double-layer repulsion. This long-range repulsion would keep the interfaces apart and delay the dewetting on the receding side (Fell et al., 2011). Thus the resulting gradient in surface tension would slow down the drainage of the liquid film.

To conclude, the mentioned simple theoretical models in their present form are not applicable to describe the three-phase contact line expansion. In the case of pure liquids, they are not able to incorporate the asymmetry of the liquid film rupture leading to bubble shape oscillations. In the case of bubble adhesion in surfactant solutions, the models do not consider the dynamic surface tension and the surfactant concentration gradient near the moving TPC line.

4. Conclusions

Bubble adhesion on a hydrophobic surface is significantly influenced by the bubble shape oscillations, which are diminished by increasing surfactant concentration. Firstly, the rupture of a liquid film is not symmetrical with respect to the vertical axis of the bubble symmetry. This asymmetry of the TPC line formation leads to bubble surface oscillations both in vertical and horizontal directions and also causes the asymmetry in dynamic contact angles. Furthermore, a non-linearity of the expansion velocity profile was observed. In pure water, i.e. in the case of full bubble surface mobility, the velocity of the three-phase contact line expansion first decreases. Due to the oscillations and kinetic energy dissipation, the second velocity maximum arises after few milliseconds. In surfactant solutions, the arising Marangoni stresses should be taken into account because the expansion velocity increases in the first moments of the TPC line expansion. Theoretical models, such as the hydrodynamic and the molecular-kinetic models are not able to incorporate the bubble oscillations in pure liquids and the non-monotonic curve of the expansion velocity profile in surfactant solutions.

References

BASAROVA, P., SUCHANOVA, H., SOUSKOVA, K., VACHOVA, T., 2017. *Bubble adhesion on hydrophobic surfaces in solutions of pure and technical grade ionic surfactants*. Colloid Surf. A, 522, 485-493.

BLAKE, T.; HAYNES, J., 1969. *Kinetics of Liquid/Liquid Displacement*. J. Colloid Interface Sci., 30, 421-423.

CHAN, D.Y.C., KLASEBOER, E., MANICA, 2011. *Film drainage and coalescence between deformable drops and bubbles*. Soft Matter, 7, 2235-2264.

COX, R.G., 1986. *The dynamics of the spreading of liquids on a solid surface. Part 1. Viscous flow*. J . Fluid Mech., 168, 169-194.

FELL, D., AUERNHAMMER, G., BONACCURSO E., LIU, C., SOKULER, R., BUTT H-J., 2011. *Influence of surfactant concentration and background salt on forced dynamic wetting and dewetting*. Langmuir, 27, 2112–2117.

FETZER, R.; RALSTON, J., 2009. *Dynamic Dewetting Regimes Explored*. J. Phys. Chem. C, 113, 8888-8894.

FUJASOVA-ZEDNIKOVA, M.; VOBECKA, L.; VEJRAZKA, J., 2010. *Effect of solid material and surfactant presence on interactions of bubbles with horizontal solid surface*. Can. J. Chem. Eng., 88, 473-481.

HUBICKA, M., BASAROVA, P., VEJRAZKA, J., 2013. *Collision of a small rising bubble with a large falling particle*. Int. J. Miner. Process., 121, 21–30.

KRASOWSKA, M., MALYSA, K., 2007. *Wetting films in attachment of the colliding bubble*. Adv. Colloid Interface Sci., 134–135, 138–150.

MALYSA, K., KRASOWSKA, M., KRZAN, M., 2005. *Influence of surface active substances on bubble motion and collision with various interfaces*. Adv. Colloid Interface Sci., 114–115, 205–225.

PHAN, C. M., NGUYEN, A. V., EVANS, G. M., 2003. *Assessment of Hydrodynamic and Molecular-Kinetic Models Applied to the Motion of the Dewetting Contact Line between a Small Bubble and a Solid Surface*. Langmuir, 19, 6796-6801.

PHAN, C. M., NGUYEN, A. V., EVANS, G. M., 2006. *Combining hydrodynamics and molecular kinetics to predict dewetting between a small bubble and a solid surface*. J. Colloid Interface Sci., 296, 669-676.

RANABOTHU, S. R., KARNEZIS, C., DAI, L. L., 2005. *Dynamic wetting: Hydrodynamic or molecular-kinetic?*. J. Colloid Interface Sci., 288, 213-221.

SCHNEEMILCH, M., HAYES, R., PETROV, J., RALSTON, J., 1998. *Dynamic wetting and dewetting of a low-energy surface by pure liquids*. Langmuir, 14, 7047-7051.

VEJRAZKA, J., VOBECKA, L., TIHON, J., 2013. *Linear oscillations of a supported bubble or drop*. Physics of Fluids, 25, 062102.

YOON, R.-H., 2000. *The role of hydrodynamic and surface forces in bubble particle interaction*. Int. J. Miner. Process., 58, 129-143.

ZAWALA, J., KOSIOR, D., DABROS, T., MALYSA, K., 2016. *Influence of bubble surface fluidity on collision kinetics and attachment to hydrophobic solids*. Colloid Surf. A, 505, 47-55.